ASTFE
American Society
of Thermal and Fluids Engineers

9th Thermal and Fluids Engineering Conference (TFEC)
April, 21-24, 2024
Partially Online Virtual and at Oregon State University, OR

TFEC-2024-50704

SUBGRID MODELING OF REACTION-RATE USING A MULTI-SCALE STRATEGY FOR LARGE-EDDY SIMULATION OF TURBULENT PREMIXED FLAMES

R. Smith,[1,*] T. Elliott,[1] R. Ranjan[1]

[1]Department of Mechanical Engineering
The University of Tennessee Chattanooga
615 McCallie Ave, Chattanooga, TN, USA 37403

ABSTRACT

In this study, we examine the performance of a multi-scale model for large-eddy simulation (LES) of turbulent premixed flames. The model referred to as RRLES performs the closure of the filtered reaction-rate term in the species transport equation while performing LES by using the linear eddy mixing (LEM) model. The RRLES model uses a multi-scale strategy to obtain the filtered reaction rate of the species and has been shown to address some of the challenges associated with the well-established LEMLES approach. The originally proposed RRLES strategy used a multilevel adaptive mesh refinement (AMR) framework, which was extended to use a single grid-based strategy to enable the application to complex geometries. Additionally, a local dual-resolution grid strategy has also been developed, which can potentially be used with different grid topologies, without the need for the AMR. We assess the accuracy and efficiency of the dual-grid RRLES approach by considering a freely propagating turbulent premixed flame under two different initial conditions corresponding to the thin reaction zone (TRZ) and the broken/distributed reaction zone (B/DRZ) regimes.

KEY WORDS: Large-eddy simulation, linear-eddy mixing model, turbulent premixed flame

Contents

*Corresponding R. Smith: nbh188@mocs.utc.edu

1. INTRODUCTION

Turbulent premixed combustion is observed in several energy conversion and propulsion applications such as gas turbines, spray combustors, aero and automotive engines, etc. Therefore, an improved understanding of flame-turbulence interactions is key to the development of novel or improvement of existing applications. Such devices are usually operated at intense turbulent conditions, however, there can be significant spatial and temporal variations in the characteristics of flame-turbulence interactions. Such interactions comprise an interplay of unsteady and nonlinear processes, which are of a multi-scale nature [23]. For example, large-scale processes include stretching/wrinkling of the flame surface by the turbulent eddies, the small-scale processes include molecular and turbulent mixing and chemical reactions, and the coupling of small and large-scale processes occur in the form of the effect of volumetric expansion due to heat-release from combustion. Therefore, computational modeling of turbulent combustion should account for such processes. Large-eddy simulation (LES), where large-scale reacting flow features are resolved by the computational grid and the effects of unresolved flow features are parametrized by employing subgrid-scale (SGS) closure, is a promising approach for the study of practical applications [7, 11, 24, 25]. However, there are several challenges with LES of reacting flows that need to be addressed so that predictive studies can be carried out in a computationally affordable and reliable manner. Some of these challenges include efficient handling of finite-rate kinetics effects, accurate modeling of thermodynamics and transport, accounting for flame-turbulence interactions under different regimes and modes of combustion, etc. In the present study, we examine the capabilities of a multi-scale strategy for LES of turbulent premixed flames under low and intense turbulent conditions.

A major focus of turbulent combustion modeling is on the closure of the filtered reaction-rate term in the governing equations [7, 11, 24, 25]. Although there exists a wide range of SGS models for turbulent combustion, there are challenges in terms of their regime of applicability, the ability to account for finite-rate kinetics effects, handling of different modes of turbulent combustion (premixed and non-premixed), handling of different regimes of turbulent premixed flames, the ability to capture ignition and extinction, etc. These challenges have lead to the development of numerous closures such as partially stirred reactor (PaSR) [7], thickened flame model (TFM) [3], flame surface density (FSD) [1], conditional moment closure (CMC) [16], conditional source estimation (CSE) [30], transported probability density function (PDF) [4, 9], multi-environment PDF (MEPDF) [6], one-dimensional turbulence (ODT) [5], and linear-eddy mixing (LEM) [19, 21] and its variants [22, 27], etc. Here, we focus on the assessment of a multi-scale model for LES, referred to as RRLES where the subgrid reaction-rate closure is attained using LEM.

The RRLES approach [27] is a modification of the well-known LEMLES approach [19], where a multi-scale strategy is used to obtain the filtered reaction rate term. The filtered LES equations are evolved on a three-dimensional (3D) grid and at every LES time step, the filtered species mass fractions and the filtered temperature fields are used to reconstruct SGS variation on the one-dimensional (1D) notional LEM domain inside each LES cell. After solving for the subgrid reaction-diffusion equation and including the effect of turbulent mixing on the 1D LEM domain, the filtered reaction rates are computed and projected back to the 3D grid. The originally proposed RRLES strategy used a multilevel adaptive mesh refinement (AMR) framework. The approach was extended to use a single grid-based strategy to enable the application to complex geometries

[22]. Recently, a local dual grid-based strategy has also been developed, which can potentially be used with different grid topologies, without the need for an AMR [26]. In the present study, we focus on the assessment of the single- and dual-grid approaches for the simulation of turbulent premixed flames.

We consider two temporally evolving freely propagating methane/air flames with one corresponding to the thin reaction zone (TRZ) regime and the other corresponding to the broken/distributed reaction zone (B/DRZ) regime based on the initial conditions. Note that turbulent premixed flames can be classified into wrinkled flamelets (WF), corrugated flamelets (CF), thin reaction zone (TRZ), and broken/distributed reaction zone (B/DRZ) [23, 25] regimes based on the length- and velocity-scale ratios corresponding to turbulence and laminar flame properties. In general, the simulation of practically relevant TRZ and B/DRZ flames is considered challenging, and therefore, flames in these regimes are considered here for the model evaluation.

This article is arranged as follows. Section 2 describes the governing equations and the subgrid closure formulations that are considered in this study. The numerical methodology and computational setup are presented in Sec. 3. The discussion of results is presented in Sec. 4. Finally, the outcomes of this study and future outlook are discussed in Sec. 5.

2. MATHEMATICAL FORMULATION

In this section, we first describe the governing equations. Afterward, we describe the SGS closure models employed in this study.

2.1 Governing equations

The LES equations are obtained by spatially filtering the compressible multi-species Navier–Stokes equations using a top-hat Favre filter, appropriate for finite volume schemes [31]. Here, $\overline{f}$ is the spatially filtered quantity for a field variable f, and $\widetilde{f} = \overline{\rho f}/\overline{\rho}$ is the Favre-filtered quantity where ρ represents the density. The filtered LES equations can be written as:

$$\frac{\partial \overline{\rho}}{\partial t} + \frac{\partial \overline{\rho}\widetilde{u_i}}{\partial x_i} = 0, \tag{1}$$

$$\frac{\partial \overline{\rho}\widetilde{u_i}}{\partial t} + \frac{\partial}{\partial x_j}[\overline{\rho}\widetilde{u_i}\widetilde{u_j} + \overline{P}\delta_{ij} - \overline{\tau}_{ij} + \tau_{ij}^{\mathrm{sgs}}] = 0, \tag{2}$$

$$\frac{\partial \overline{\rho}\widetilde{E}}{\partial t} + \frac{\partial}{\partial x_i}[(\overline{\rho}\widetilde{E} + \overline{P})\widetilde{u_i} + \overline{q}_i - \widetilde{u_j}\overline{\tau}_{ij} + H_i^{\mathrm{sgs}} + \sigma_i^{\mathrm{sgs}}] = 0, \tag{3}$$

$$\frac{\partial \overline{\rho}\widetilde{Y_k}}{\partial t} + \frac{\partial}{\partial x_i}[\overline{\rho}(\widetilde{Y_k}\widetilde{u_i} + \widetilde{Y_k}\widetilde{V}_{i,k}) + y_{i,k}^{\mathrm{sgs}} + \theta_{i,k}^{\mathrm{sgs}}] = \overline{\dot{\omega}}_k \quad k = 1, ..., N_s. \tag{4}$$

Here, ρ is the density, $(u_i)_{i=1,2,3}$ is the velocity vector in Cartesian coordinates, T is the temperature, P is the pressure, and Y_k is the mass fraction for the k^{th} species. Additionally, N_s is the total number of species in the flow. The total energy in the system is the sum of the internal energy and the kinetic energy. As a result, the filtered total energy is presented as a sum of the filtered internal energy $(\widetilde{e})$, the resolved kinetic energy $(\frac{1}{2}[\widetilde{u_i}\widetilde{u_j}])$, and the subgrid kinetic energy $(k^{\mathrm{sgs}} = \frac{1}{2}[\widetilde{u_i u_i} - \widetilde{u_i}\widetilde{u_i}])$. The thermally perfect gas equation of state is used to close the equations as $\overline{P} = \overline{\rho}(\widetilde{R}\widetilde{T} + T^{\mathrm{sgs}})$. The filtered viscous stress tensor and the filtered heat-flux vector are approximated as:

$$\overline{\tau}_{ij} = 2\mu(\widetilde{T})(\widetilde{S}_{ij} - \frac{1}{3}\widetilde{S}_{kk}\delta_{ij}), \tag{5}$$

$$\overline{q}_i = -k(\widetilde{T})\frac{\partial \widetilde{T}}{\partial x_i} + \overline{\rho}\sum_{k=1}^{N_s}\widetilde{h}_k\widetilde{Y}_k\widetilde{V}_{i,k} + \sum_{k=1}^{N_s} q_{i,k}^{\text{sgs}}, \tag{6}$$

where $\widetilde{S}_{ij} = \frac{1}{2}(\frac{\partial \widetilde{u}_i}{\partial x_j} + \frac{\partial \widetilde{u}_j}{\partial x_i})$ is the resolved rate of strain. The filtered diffusion velocity for the k^{th} species is modeled as

$$\widetilde{V}_{i,k} = -\overline{D}_k\frac{\partial \widetilde{X}_k}{\partial x_i} + \frac{1}{W}\sum_{k=1}^{N_s}\overline{D}_k W_k\frac{\partial X_k}{\partial x_i}, \tag{7}$$

where W is the mixture molecular weight, and $\overline{D}_k$ and $\widetilde{X}_k$ are the diffusion coefficient and mole fraction of the k_{th} species, respectively. The diffusion coefficient for a species is obtained through the well-known mixture-averaged formulation [25].

All of the subgrid-scale terms, denoted with a "sgs" superscript, are unclosed, and therefore, require specific modeling. These terms are:

$$\tau_{ij}^{\text{sgs}} = \overline{\rho}(\widetilde{u_i u_j} - \widetilde{u}_i\widetilde{u}_j), \tag{8}$$

$$H_i^{\text{sgs}} = \overline{\rho}(\widetilde{Eu_i} - \widetilde{E}\widetilde{u}_i) + (\overline{u_i P} - \widetilde{u}_i\overline{P}), \tag{9}$$

$$\sigma_i^{\text{sgs}} = (\overline{u_j\tau_{ij}} - \widetilde{u}_j\overline{\tau}_{ij}), \tag{10}$$

$$\mathcal{Y}_{i,k}^{\text{sgs}} = \overline{\rho}(\widetilde{u_i Y_k} - \widetilde{u}_i\widetilde{Y}_k), \tag{11}$$

$$\theta_{i,k}^{\text{sgs}} = \overline{\rho}(\widetilde{Y_k V}_{i,k} - \widetilde{Y}_k\widetilde{V}_{i,k}), \tag{12}$$

$$q_{i,k}^{\text{sgs}} = \overline{\rho}(h_k\widetilde{Y_k V}_{i,k} - \widetilde{h}_k\widetilde{Y}_k\widetilde{V}_{i,k}), \tag{13}$$

$$T^{\text{sgs}} = \widetilde{RT} - \widetilde{R}\widetilde{T}, \tag{14}$$

$$E_k^{\text{sgs}} = \widetilde{Y_k e_k(T)} - \widetilde{Y}_k e_k(\widetilde{T}). \tag{15}$$

The governing equations are complete after specifying closure models for the SGS terms, and initial and boundary conditions for the specific problem. Next, we briefly describe the subgrid models.

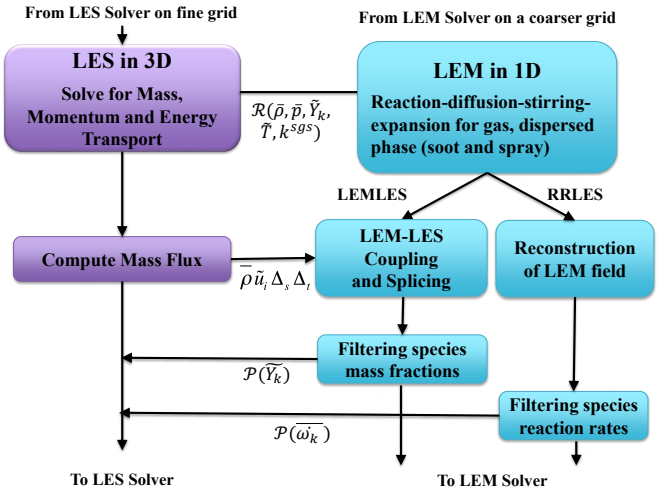

Fig. 1 A typical workflow in the LEMLES and RRLES strategies [27].

2.2 Subgrid Modeling of SGS Stress and Scalar Flux

The subgrid stress and enthalpy flux and the subgrid viscous work terms are present even in non-reacting flows, and their modeling follows past efforts relying on eddy viscosity/diffusivity formulation [10, 20]. Specifically, the unclosed subgrid stress term τ_{ij}^{sgs} is modeled as

$$\tau_{ij}^{\text{sgs}} = -2\overline{\rho}\nu_t(\widetilde{S}_{ij} - \frac{1}{3}\widetilde{S}_{kk}\delta_{ij}) + \frac{2}{3}k^{\text{sgs}}\delta_{ij}, \tag{16}$$

and the two unclosed terms in the energy equation, H_i^{sgs} and σ_i^{sgs}, are modeled together as

$$H_i^{\text{sgs}} + \sigma_i^{\text{sgs}} = (\overline{\rho}\nu_t\mu)\frac{\partial k^{\text{sgs}}}{\partial x_i} + \frac{\overline{\rho}\nu_t c_p}{Pr_t}\frac{\partial \widetilde{T}}{\partial x_i} + \widetilde{u}_j\tau_{ij}^{\text{sgs}}. \tag{17}$$

Here we employ a one-equation model for the subgrid kinetic energy [14, 20] to determine the subgrid eddy viscosity as $\nu_t = C_v\sqrt{k^{sgs}}\Delta$, where Δ is the grid filter width and C_v is a coefficient calculated using the localized dynamic kinetic energy model (LDKM) [10, 14]. Similarly, Pr_t is also determined using a locally dynamic procedure [10]. The modeling of subgrid scalar flux $\mathcal{Y}_{i,k}^{\text{sgs}}$ is obtained using an eddy diffusivity-based approach while employing the RRLES strategy. On the other hand, in LEMLES, the two-scale strategy is used to solve the scalar transport equations, and therefore, no explicit modeling of $\mathcal{Y}_{i,k}^{\text{sgs}}$ is required. Following a past study LES [8], $q_{i,k}^{\text{sgs}}$, T^{sgs} and E_k^{sgs}, are neglected in the present study. Next, we discuss the closure of the filtered reaction rate term.

2.3 Subgrid Modeling of Filtered Reaction Rate

The RRLES approach [27] is a modification of the well-known LEMLES approach [19], where the filtered reaction-rate terms ($\overline{\dot{\omega}}_k$) are modeled using a multi-scale LEM framework. At every LES time step, the filtered species mass fractions ($\widetilde{Y}_i$) and the filtered temperature ($\widetilde{T}$) evolving at the resolved 3D level are used to reconstruct SGS variation on the 1D notional LEM domain inside each LES cell, and after solving for the subgrid reaction-diffusion equation and including the effect of turbulent mixing in the 1D LEM domain, the filtered reaction rates are computed and projected back to the LES grid. A workflow of the RRLES strategy compared to LEMLES is shown in Fig. 1.

In the RRLES strategy, the first step is the reconstruction of the species mass fraction and the temperature

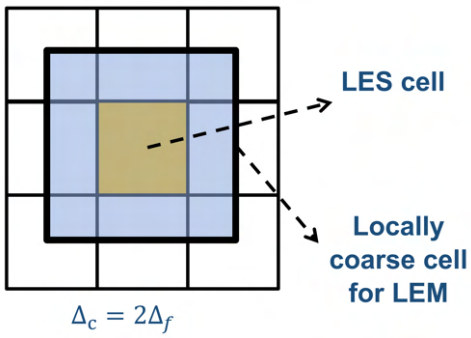

Fig. 2 Schematic of the dual-grid strategy employed in the RRLES approach.

field in the 1D LEM domain using the resolved 3D fields, which is performed as

$$Y_i^{\mathrm{LEM}}(s) = \mathcal{R}\left(\widetilde{Y}_i, \nabla\widetilde{Y}_i\right), \quad T^{\mathrm{LEM}}(s) = \mathcal{R}\left(\widetilde{T}, \nabla\widetilde{T}\right), \tag{18}$$

where, $\mathcal{R}\left(\widetilde{\phi}, \nabla\widetilde{\phi}\right) = \widetilde{\phi} - \nabla\widetilde{\phi}\Delta/2 + |\nabla\widetilde{\phi}|\Delta s$ is a gradient-based reconstruction operator, 's' represents the co-ordinate along the 1D LEM domain, and Δ represents the LES filter size. After the reconstruction step, the governing equations for the species mass-fraction and the temperature are solved on the notional 1D LEM domain inside each LES computational cell as

$$\rho\frac{\partial Y_k}{\partial t} = F_{k,\mathrm{stir}} - \frac{\partial}{\partial s}\left(\rho Y_k V_{s,k}\right) + \dot{\omega}_k, \tag{19}$$

$$\rho C_{p,\mathrm{mix}}\frac{\partial T}{\partial t} = F_{T,\mathrm{stir}} + \frac{\partial}{\partial s}\left(\kappa\frac{\partial T}{\partial s}\right) - \frac{\partial}{\partial s}\left(\sum_{k=1}^{N_s} h_i \rho Y_k V_{s,k}\right) - \sum_{k=1}^{N_s} h_k \dot{\omega}_k. \tag{20}$$

Each 1D LEM domain is discretized using N_{LEM} cells to ensure the required spatial resolution of the scalar fields. The processes involved in the subgrid evolution include molecular diffusion, turbulent transport by the unresolved eddies, chemical reaction, and thermal expansion for the species at their respective spatial and temporal scales. The terms $F_{k,\mathrm{stir}}$ and $F_{T,\mathrm{stir}}$ represent the stochastic events, which simulate the effects of turbulent mixing by the SGS eddies on the 1D LEM lines [13, 19]. Finally, after solving for the SGS variations, the filtered reaction-rate term $\overline{\dot{\omega}}_k$ is obtained for the corresponding LES cell through:

$$\overline{\dot{\omega}}_k = \frac{\sum_{m=1}^{N_{\mathrm{LEM}}} \dot{\omega}_{k,m}\Delta V_m}{\sum_{m=1}^{N_{\mathrm{LEM}}} \Delta V_m}. \tag{21}$$

The approach was extended to use a single grid-based strategy to enable the application to complex geometries [22]. Recently, a local dual grid-based strategy has also been developed, which can potentially be used with different grid topologies, without the need for an AMR [26]. We will assess the performance of both these approaches in the present study.

A schematic of the local dual-grid strategy is shown in Fig. 2. In this strategy, the LEM subgrid fields evolve on a coarser LES grid with an effective resolution $\Delta^{\mathrm{LEM}} = 2\Delta$, while the LES governing equations are still resolved on the much finer grid of resolution Δ. The coarser grid has more unresolved scales, which can potentially lead to an improved prediction by solving the 1D LEM equations. Additionally, this strategy requires consistent restriction operations for the resolved LES quantities needed by LEM.

Table 1 Simulation parameters of all cases considered in this study.

Case	Closure	$\mathbf{N_x \times N_y \times N_z}$	$\mathbf{u'/S_L}$	$\mathbf{l/\delta_L}$	**Re**	**Ka**	**Da**
A	DNS	$192 \times 192 \times 192$	10.0	0.74	62.8	36.8	0.07
	LEMLES	$64 \times 64 \times 64$	10.0	0.74	62.8	36.8	0.07
	RRLES-S	$64 \times 64 \times 64$	10.0	0.74	62.8	36.8	0.07
	RRLES	$64 \times 64 \times 64$	10.0	0.74	62.8	36.8	0.07
B	DNS	$256 \times 256 \times 256$	50.0	6.2	478.7	142.0	0.12
	LEMLES	$96 \times 96 \times 96$	50.0	6.2	478.7	142.0	0.12
	RRLES	$96 \times 96 \times 96$	50.0	6.2	478.7	142.0	0.12

3. COMPUTATIONAL APPROACH AND SETUP

In this section, the details of the numerical methodology and the computational setup for the turbulent premixed flame cases are discussed.

3.1 Numerical methodology

The governing equations described in Sec. 2.1 are solved using a well-established three-dimensional (3D) parallel, multi-species compressible reacting flow solver, referred to as AVF-LESLIE [15, 28]. It is a multi-physics simulation tool capable of performing DNS and LES of reacting/non-reacting flows in canonical and moderately complex flow configurations. It has been extensively used in the past to study a wide variety of flow conditions, including acoustic flame-vortex interaction, premixed flame turbulence interaction, non-premixed combustion, and compressible turbulence [2, 15, 17, 28, 32].

The solver utilizes a finite volume-based spatial discretization of the governing equations in their conservative form on a structured grid using the generalized curvilinear coordinates. The spatial discretization is based on the well-known second-order accurate MacCormack scheme [18]. The time integration of the semi-discrete system of equations is performed by an explicit second-order accurate scheme. The solver can handle arbitrarily complex finite-rate chemical kinetics. The mixture-averaged transport properties, the finite-rate kinetics source terms, and the thermally perfect gas-based thermodynamic properties are obtained using the Cantera software [12]. The parallelization of the solver is based on the standard domain decomposition technique based on the message-passing interface library.

3.2 Computational setup

The cases considered here correspond to the interaction of an initially premixed laminar flame with decaying isotropic turbulence. Figure 3(a) shows a schematic of the premixed planar flame configuration. The initial flame front is specified near the center of the computational domain with reactants and products on its left and right sides, respectively. The extent of the computational domain is $L_x \times L_y \times L_z$ in the streamwise, transverse, and spanwise directions, where L = 0.0055 m. The flow field is initialized using an isotropic turbulent flow field and is superimposed with a one-dimensional planar flame solution obtained at ϕ = 0.8, T_{ref} = 570 K, and P_{ref} = 1 atm. Here, ϕ denotes the equivalence ratio of the methane-air mixture, T_{ref} is the temperature on the reactants side, and P_{ref} is the reference pressure. A characteristic-based inflow-outflow boundary condition is used in the streamwise direction and a periodic boundary condition is used along the spanwise and transverse directions.

The simulation parameters for all of the cases are presented in Table 1. Here, l is the integral length scale, u' is the turbulence intensity, S_L is the laminar flame speed, and $\delta_{\mathrm{L}} = (T_b - T_u)/|\nabla T|_{max}$ is the laminar thermal flame thickness. The subscripts 'u' and 'b' denote unburnt and burnt sides of the flame respectively. Additionally, Re, Ka, and Da denote the integral Reynolds number, the Karlovitz number, and the Damköhler

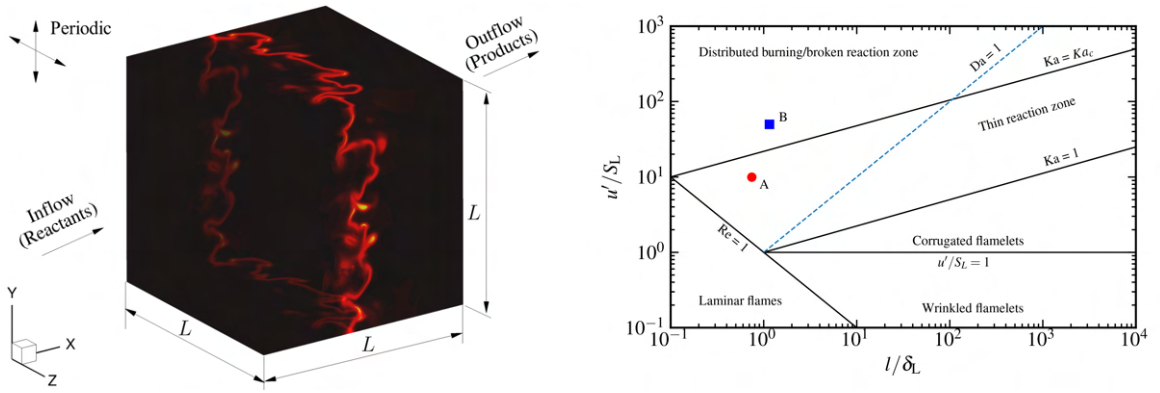

(a) (b)

Fig. 3 A schematic of the turbulent premixed flame configuration (a) and the premixed flame regime diagram [23] (b) showing the cases considered in the present study.

number, respectively. These are defined as $Re = \dfrac{u'l}{\nu}$, $Ka = \sqrt{\dfrac{u'^3\delta_{\mathrm{L}}}{S_L^3 l}}$ and $Da = \dfrac{S_L l}{u'\delta_L}$, respectively. We consider two turbulent premixed flame configurations, labeled as cases A and B. For each of these cases, we conduct simulations employing DNS, LEMLES, single-grid RRLES, and dual-grid RRLES techniques. Here onwards, the single-grid RRLES strategy is denoted by 'RRLES-S' and the dual-grid RRLES strategy is denoted by 'RRLES'. Case A corresponds to the TRZ regime and Case B corresponds to the B/DRZ regime. The regimes of the flames are characterized based on the initial conditions and these cases are shown on the regime diagram in Fig. 3(b).

The grid resolution is chosen based on previous studies, and for the conditions considered here is more than sufficient to reach $k_{\max}\eta \geq 1$ for DNS, where $k_{\max}$ is the largest wave number and η is the Kolmogorov length scale. With the grids employed in the present study, it is estimated that the thermal flame thickness, δ_{L}, is resolved by around 20 points in DNS and 5 points in LES cases. The simulations are carried out till $3t_0$, where $t_0 = l/u'$ denotes the initial eddy turnover time. Past studies have shown that 2-3 eddy turnover times are adequate for flame-turbulence interaction to evolve in the configuration considered in this study.

4. RESULTS AND DISCUSSION

In this section, we first compare single and dual-grid RRLES strategies by considering Case A. Afterward, we assess the capabilities of the dual-grid strategy to simulate the two cases by comparing with reference DNS and LEMLES results.

4.1 Comparison of Single and Dual-Grid Approaches

A comparison of some of the spatially averaged quantities for single- and dual-grid RRLES modeling strategies for Case A is shown in Fig. 4. The shown quantities include the progress variable (c), normalized heat-release rate (q^*), and the normalized mass fraction of the intermediate species ($Y^*_{\mathrm{H_2}}$). Here, c is defined based on the mass fraction of the fuel as

$$c = \frac{Y_{\mathrm{CH_{4,u}}} - Y_{\mathrm{CH_4}}}{Y_{\mathrm{CH_{4,u}}} - Y_{\mathrm{CH_{4,b}}}}. \tag{22}$$

The value of c varies from 0 in the fresh reactants to 1 in the burned products. The normalization of heat-release rate and mass fraction of $\mathrm{H_2}$ is performed using the peak value of these quantities of the corresponding

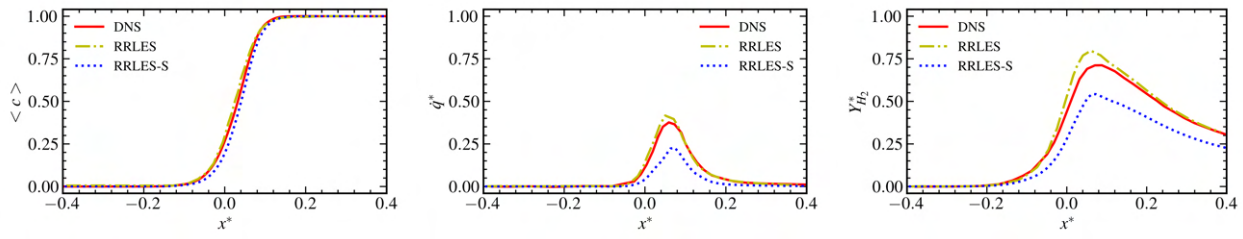

(a) (b) (c)

Fig. 4 Streamwise profile of the spatially averaged progress variable (a), normalized heat release rate (b), and normalized mass fraction of H_2 (c) comparing single- and dual-grid RRLES strategies for Case A.

laminar premixed flame. The spatial averaging of a quantity ψ is performed along the homogeneous y- and z-directions through

$$\langle \psi \rangle(x,t) \equiv \frac{1}{L^2} \int_0^L \int_0^L \psi(x,y,z,t)\, dy\, dz. \tag{23}$$

The variation of $\langle c \rangle$ along the streamwise direction shows a broadening of the flame brush. We observe that both single- and dual-grid RRLES approaches show a good agreement with DNS, with the dual-grid strategy showing marginally better agreement. However, the effect of single- and dual-grid approaches is apparent from the streamwise variation of heat-release rate and the intermediate species. The single-grid RRLES tends to under-predict q^* and $Y^*_{H_2}$, whereas the dual-grid RRLES show a very good agreement with the reference DNS results.

4.2 Application of Dual-Grid RRLES

Now, we employ the dual-grid RRLES to examine its capabilities to simulate flames in different regimes. We compare the performance of the RRLES strategy with respect to DNS and LEMLES approaches.

4.2.1 Structural features of flames The flame structure and its characteristics are assessed using the progress variable c. Following past studies [28, 29], we identify a notional flame surface by an iso-level of $c = 0.8$ and the bounds of the flame brush correspond to $c \in [0.01, 0.99]$. While comparing LEMLES and RRLES predictions, the filtered progress variable $\widetilde{c}$ is defined in a way similar to Eq. 22 but using the filtered mass fraction of the fuel.

Figure 5 shows the instantaneous structure of the flame brush obtained from DNS for the two cases. We can observe intense wrinkling and stretching of the initially planar flame surface by the turbulent eddies. The effect of heat release and associated thermal expansion across the flame is apparent in terms of an increase in the overall length scales associated with the protruding structures on both the reactants and the products sides. Turbulent eddies sustain the flame by transporting pockets of cold reactants toward the reaction zone. In both cases, the flame structure is continuous, thus precluding the presence of any local extinction. We also observe the spatial broadening of the flames along the streamwise direction, where the broadening is higher in Case B due to a higher value of Ka in this case [22, 27].

Figure 6 compares the flame structure obtained from DNS, LEMLES and RRLES for the two cases in the central $x - y$ plane. Qualitatively, the wrinkling and stretching of the flame surface is captured by both LEMLES and RRLES approaches in a manner similar to the DNS cases. Furthermore, the increased flame broadening and increased amount of wrinkling in Case B due to a higher Ka is also captured by the two closure models. However, there are observable differences as well. Similar to DNS, the RRLES results show fine-scale grid-resolved wrinkling, which is not evident in the LEMLES cases. This can be attributed to the

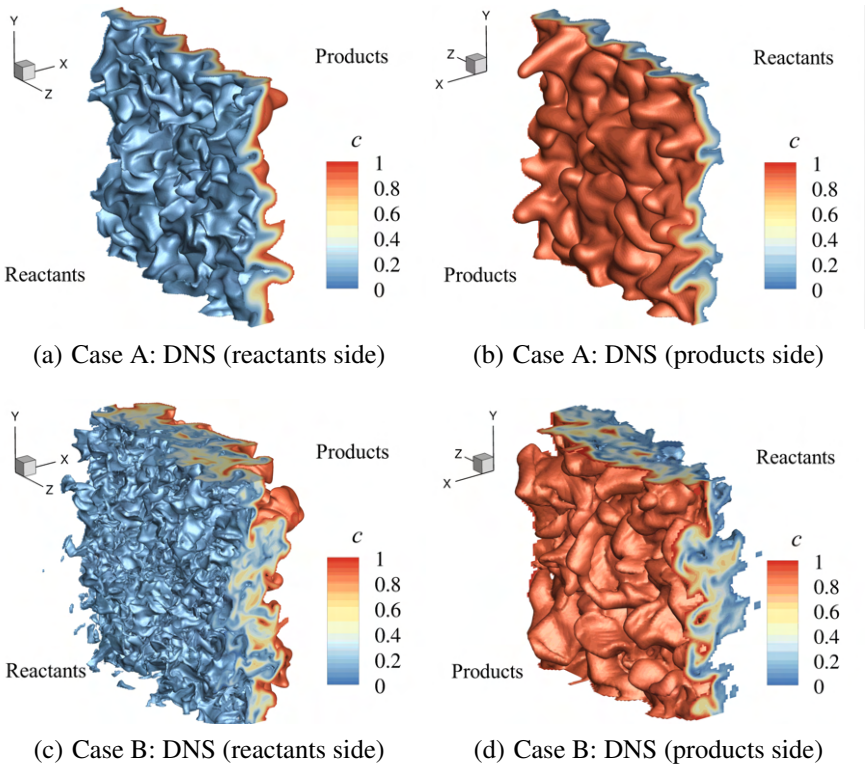

(a) Case A: DNS (reactants side) (b) Case A: DNS (products side)

(c) Case B: DNS (reactants side) (d) Case B: DNS (products side)

Fig. 5 Structure of the flame brush from cases A (a, b) and B (c, d) obtained using DNS.

way scalar fields are evolved in the RRLES and LEMLES approaches. While in the resolved scalar field corresponds to the resolved value of the corresponding LEM field on the LES grid, in the RRLES formulation the resolved scalar field is explicitly solved. Additionally, in Case A, the spatial variation of temperature tends to be diffused. This is associated with the limitations of LEMLES in accurately capturing features of low Re flame, where RRLES tends to perform better. This is discussed next quantitatively in terms of spatially and conditionally averaged statistics of thermo-chemical quantities.

4.2.2 Flame statictics The streamwise profile of several spatially averaged quantities is shown in Fig. 7 comparing LEMLES and RRLES with corresponding DNS cases. We observe the effect of turbulence in both cases, as due to the spatial broadening of the flames, the spatially averaged profile in both cases differs from the corresponding laminar flame profiles. As expected, in the low Ka case, i.e., Case A, LEMLES does not perform well. In particular, the heat-release rate and the mass fraction of the intermediate species, i.e., H_2 are under-predicted compared to DNS. However, RRLES shows a good agreement with the DNS results for this case. This illustrates that the blending employed by the dual-grid RRLES formulation allows it to include contributions from LEM at the subgrid level as the turbulence level increases and with a decrease in turbulence level it takes contributions from the quasi-laminar chemistry. At the higher value of Ka, i.e., in Case B, the performance of LEMLES tends to improve, which is expected. On the other hand, RRLES tends to yield a reasonable agreement, where we observe an over-prediction of the peak heat release rate and the mass fraction of H_2.

To assess the performance of LEMLES and RRLES, we examine the state-space variation of thermo-chemical quantities, which is shown in Fig. 8 for all cases. Similar to the spatially averaged profile shown in Fig. 7, the conditionally averaged profiles in both cases tend to differ from the corresponding laminar flames. The differences are much more apparent in the variation of $\dot{q}^*$ and $Y^*_{H_2}$. Furthermore, similar to the spatially averaged profile shown in Fig. 7, the asymptotic behavior of the RRLES closure is evident here, as we can

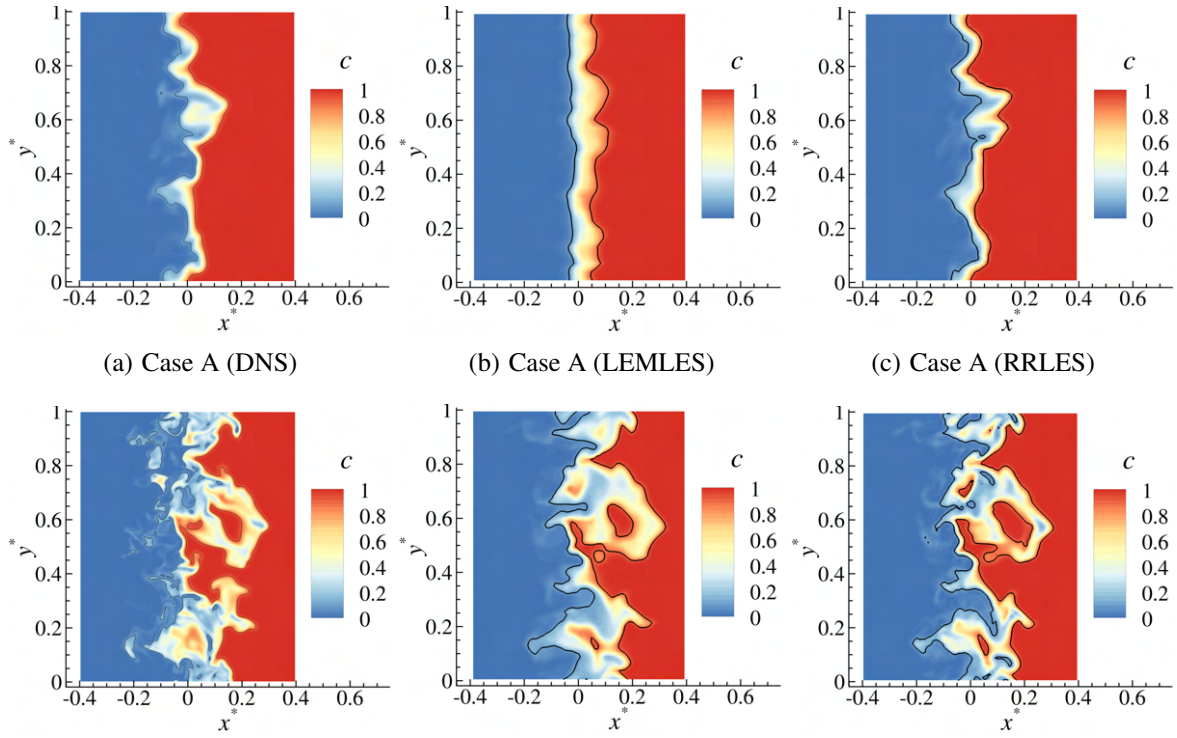

(a) Case A (DNS) (b) Case A (LEMLES) (c) Case A (RRLES)

(d) Case B (DNS) (e) Case B (LEMLES) (f) Case B (RRLES)

Fig. 6 Contours of filtered temperature field overlaid with the flame brush extents in the central $x - y$ plane obtained using DNS (a, d), LEMLES (b, e), and RRLES (c, f) approaches for cases A (a, b, c) and B (d, e, f).

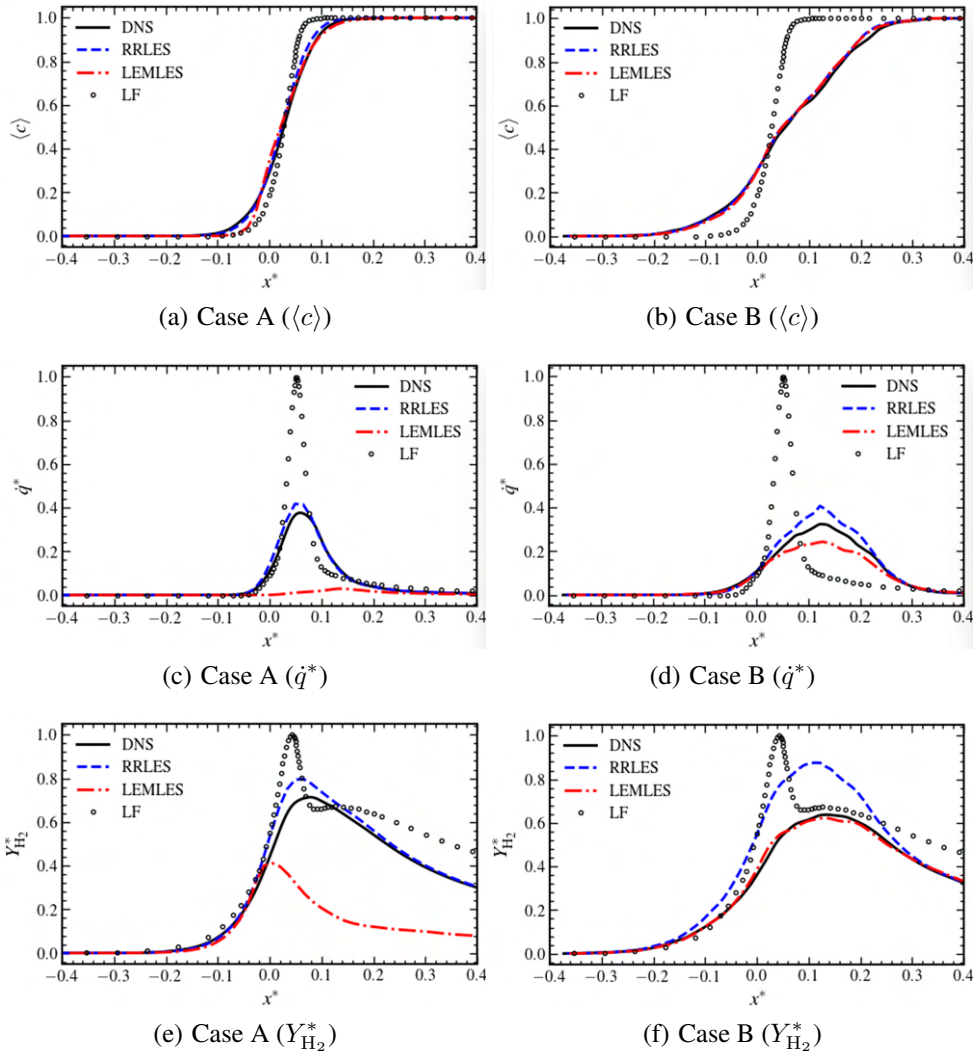

(a) Case A ($\langle c \rangle$) (b) Case B ($\langle c \rangle$)

(c) Case A ($\dot{q}^*$) (d) Case B ($\dot{q}^*$)

(e) Case A ($Y^*_{H_2}$) (f) Case B ($Y^*_{H_2}$)

Fig. 7 Streamwise profile of the spatially averaged progress variable (a, b), normalized heat release rate (c, d), and normalized mass fraction of H_2 (e, f) from cases A (a, c, e) and B (b, d, f). The curves labeled as 'LF' corresponds to results from laminar flame.

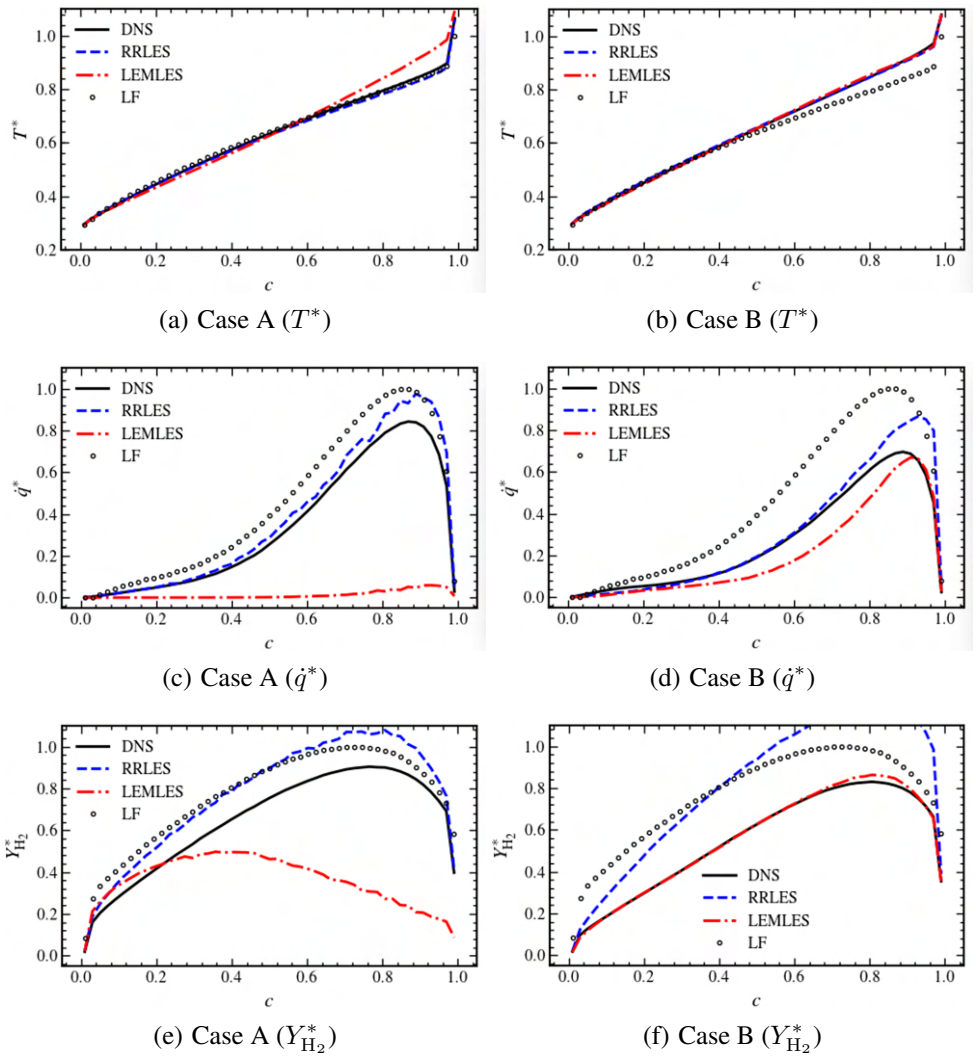

(a) Case A (T^*) (b) Case B (T^*)

(c) Case A ($\dot{q}^*$) (d) Case B ($\dot{q}^*$)

(e) Case A ($Y^*_{H_2}$) (f) Case B ($Y^*_{H_2}$)

Fig. 8 Conditionally averaged normalized temperature (a, b), normalized heat release rate (c, d), and normalized mass fraction of H_2 (e, f) with respect to the progress variable from cases A (a, c, e) and B (b, d, f). The curves labeled as 'LF' corresponds to results from laminar flame.

observe that its prediction approaches DNS when the turbulence level is relatively lower in Case A compared to Case B. Here, we again see the limitations of the LEMLES approach in Case A when the local flow conditions have low subgrid-scale turbulence due to lower Ka and Re. But in the higher Ka case, i.e., Case B, LEMLES tend to approach DNS results, while RRLES approach exhibits over-prediction of $\dot{q}^*$ and $Y^*_{\mathrm{H_2}}$.

The quantitative results discussed in this section illustrate that RRLES tend to yield an overall good agreement with the DNS in capturing the flame structure of both cases. However, further improvements can be performed in the RRLES closure to improve accuracy in the results for the high Ka case.

5. CONCLUSIONS

LES is a promising strategy for the numerical investigation of turbulent premixed combustion. However, accurate and reliable SGS models are needed to enable predictive studies of turbulent premixed combustion observed in practically relevant configurations where spatial and temporal variations can lead to different regimes of premixed combustion. In the present study, we assess the capabilities of a multi-scale strategy, referred to as RRLES, to capture features of turbulent premixed flames. In RRLES, the filtered reaction rate is obtained by solving scalar transport equations at the subgrid level using the LEM model. The model addresses some of the challenges associated with the well-established LEMLES strategy, particularly, in capturing flame-turbulence interactions prevalent at low to moderate Re.

The RRLES strategy was originally established using an AMR framework, where the flow field equations are solved on a fine grid and the scalar equations are solved on a coarse grid to enable effective contributions by the subgrid LEM model. The approach was also extended to a single-grid strategy to allow for the simulation of complex geometries using solvers that do not have AMR capability. It was later extended to allow for a locally dual-grid strategy so that AMR is not needed while the effectiveness of the subgrid LEM model is still retained. In the present study, we assessed the capabilities of the single and dual-grid RRLES strategies and then examined dual-grid RRLES for the simulation of turbulent premixed flames from two different regimes. We simulated methane/air freely propagating and temporally evolving turbulent premixed flames in the TRZ and B/DRZ regimes to assess the capabilities of the RRLES strategies.

The dual-grid strategy showed improved agreement of the spatially-averaged flame structure with the DNS results compared to the single-grid strategy. Additionally, the dual-grid strategy also showed an improved agreement with the DNS for the low Re and low Ka case and a reasonable agreement with the DNS for the high Re and high Ka case. The results illustrated the robustness of the dual-grid RRLES in capturing features of turbulent premixed flames in different regimes. Future studies will focus on assessing the capabilities of RRLES for the simulation of turbulent non-premixed flames and attaining closure of some of the terms that are neglected at the resolved level in the present study.

ACKNOWLEDGMENTS

Dr. Ranjan acknowledges the support of National Science Foundation (NSF) (Grant #: 2301829 , Program Officer: Dr. Harsha Chelliah). Mr. Smith was supported in part by a CEACSE grant through the University of Tennessee Chattanooga (UTC). The computational resources were provided by the UTC Research Institute under grants from the National Science Foundation (Grant Nos. 1925603 and 2201497) and are greatly appreciated.

REFERENCES

[1] Boger, M., Veynante, D., Boughanem, H., and Trouve, A., (1998) "Direct numerical simulation analysis of flame surface density concept for large eddy simulation of turbulent premixed combustion," *Proc. Combust. Inst.*, 27, pp. 917–925.

[2] Bowers, J., Durant, E., and Ranjan, R., (2021) "Application of intrusive and non-intrusive reduced order modeling techniques for simulation of turbulent premixed flames," *AIAA Propulsion and Energy 2021 Forum*, p. 3634.

[3] Colin, O., Ducros, F., Veynante, D., and Poinsot, T., (2000) "A thickened flame model for large eddy simulations of turbulent premixed combustion," *Phys. of Fluids*, 12(7), pp. 1843–1863.

[4] Colucci, P., Jaberi, F., Givi, P., and Pope, S., (1998) "Filtered density function for large eddy simulation of turbulent reacting flows," *Phys. of Fluids*, 10(2), pp. 499–515.

[5] Echekki, T., Kerstein, A. R., Dreeben, T. D., and Chen, J.-Y., (2001) "?one-dimensional turbulence? simulation of turbulent jet diffusion flames: model formulation and illustrative applications," *Comp. and Fluids*, 125(3), pp. 1083–1105.

[6] Fox, R. O. and Raman, V., (2004) "A multienvironment conditional probability density function model for turbulent reacting flows," *Phys. of Fluids*, 16(12), pp. 4551–4565.

[7] Fureby, C., (2009) "Large eddy simulation modelling of combustion for propulsion applications," *Philosophical Transactions of the Royal Society A: Mathematical, Physical and Engineering Sciences*, 367(1899), pp. 2957–2969.

[8] Fureby, C. and Möller, S.-I., (1995) "Large eddy simulation of reacting flows applied to bluff body stabilized flames," *AIAA J.*, 33(12), pp. 2339–2347.

[9] Gao, F. and O'Brien, E. E., (1993) "A large-eddy simulation scheme for turbulent reacting flows," *Phys. of Fluids*, 5, pp. 1282–1284.

[10] Génin, F. and Menon, S., (2010) "Studies of shock/turbulent shear layer interaction using Large-Eddy Simulation," *Computers & Fluids*, 39, pp. 800–819.

[11] Gonzalez-Juez, E. D., Kerstein, A. R., Ranjan, R., and Menon, S., (2017) "Advances and challenges in modeling high-speed turbulent combustion in propulsion systems," *Prog. Energy Combust. Sci.*, 60, pp. 26–67.

[12] Goodwin, D. G., Moffat, H. K., and Speth, R. L., (2014) "Cantera: An object-oriented software toolkit for chemical kinetics, thermodynamics, and transport processes," , , `http://www.cantera.org`, version 2.1.2.

[13] Kerstein, A. R., (1989) "Linear-eddy modeling of turbulent transport. II: Application to shear layer mixing," *Combust. Flame*, 75(3-4), pp. 397–413.

[14] Kim, W. W. and Menon, S., (1999) "An unsteady incompressible Navier-Stokes solver for large eddy simulation of turbulent flows," *I. J. for Numer. Meth. Fluids.*, 31(6), pp. 983–1017.

[15] Kim, W.-W. and Menon, S., (2000) "Numerical modeling of turbulent premixed flames in the thin-reaction-zones regime," *Combust. Sci. Technol.*, 160(1), pp. 119–150.

[16] Klimenko, A. Y. and Bilger, R. W., (1999) "Conditional moment closure for turbulent combustion," *Prog. Energy Combust. Sci.*, 25(6), pp. 595–687.

[17] Lowery, C., Hasti, V. R., and Ranjan, R., (2022) "Characteristics of non-equilibrium turbulence in couette flow under compressible conditions," *AIAA AVIATION 2022 Forum*, p. 4035.

[18] MacCormack, R. W., (2003) "The effect of viscosity in hypervelocity impact cratering," *J. Space. Rockets*, 40(5), pp. 757–763.

[19] Menon, S. and Kerstein, A. R., (2011) "The linear-eddy model," *Turbulent Combustion Modeling*, 95, pp. 175–222.

[20] Menon, S. and Kim, W., (1996) "High Reynolds number flow simulations using the localized dynamic subgrid-scale model," *AIAA paper*, 425, pp. 1996.

[21] Menon, S., McMurtry, P., and Kerstein, A. R., (1993) "A linear eddy mixing model for large eddy simulation of turbulent combustion," , *LES of Complex Engineering and Geophysical Flows*. Galperin, B. and Orszag, S. (Eds.). Cambridge University Press, pp. 287–314.

[22] Panchal, A., Ranjan, R., and Menon, S., (2019) "A comparison of finite-rate kinetics and flamelet-generated manifold using a multiscale modeling framework for turbulent premixed combustion," *Combustion Science and Technology*, 191(5-6), pp. 921–955.

[23] Peters, N., (2000) *Turbulent Combustion*, Cambridge University Press.

[24] Pitsch, H., (2006) "Large-eddy simulation of turbulent combustion," *Annu. Rev. Fluid Mech.*, 38, pp. 453–482.

[25] Poinsot, T. and Veynante, D., (2005) *Theoretical and Numerical Combustion*, 2nd Edition, Edwards, Inc.

[26] Ranjan, R., (2021) "A dual grid strategy for subgrid reaction-rate closure using linear eddy mixing model for large-eddy simulation of turbulent combustion," *APS Division of Fluid Dynamics Meeting Abstracts*, pp. H09–003.

[27] Ranjan, R., Muralidharan, B., Nagaoka, Y., and Menon, S., (2016) "Subgrid-scale modeling of reaction-diffusion and scalar transport in turbulent premixed flames," *Combust. Sci. Technol.*, 188, pp. 1496–1537.

[28] Sankaran, V. and Menon, S., (2005) "Subgrid combustion modeling of 3-D premixed flames in the thin-reaction-zone regime," *Proc. Combust. Inst.*, 30(1), pp. 575–582.

[29] Savre, J., Carlsson, H., and Bai, X. S., (2013) "Turbulent methane/air premixed flame structure at high Karlovitz numbers," *Flow Turbulence Combust.*, 90(2), pp. 325–341.

[30] Steiner, H. and Bushe, W., (2001) "Large eddy simulation of a turbulent reacting jet with conditional source-term estimation," *Phys. of Fluids*, 13(3), pp. 754–769.

[31] Vreman, B., Geurts, B., and Kuerten, H., (1994) “On the formulation of the dynamic mixed subgrid-scale model,” *Phys. of Fluids*, 6, pp. 4057–4059.

[32] Yang, S., Ranjan, R., Yang, V., Wenting, S., and Menon, S., (2017) “Sensitivity of predictions to chemical kinetics models in a temporally evolving turbulent non-premixed flame,” *Combustion and Flame*, 183, pp. 224–241.